

# JWST telescope integration and test progress

Gary W. Matthews<sup>a</sup>, Tony L. Whitman<sup>a</sup>, Lee D. Feinberg<sup>b</sup>, Mark F. Voyton<sup>b</sup>, Juli A. Lander<sup>b</sup>,  
Ritva Keski-Kuha<sup>b</sup>

<sup>a</sup>Harris (United States), <sup>b</sup>NASA Goddard Space Flight Center (United States)

## ABSTRACT

The James Webb Space Telescope (JWST) is a 6.5m, segmented, IR telescope that will explore the first light of the universe after the big bang. The JWST Optical Telescope Element (Telescope) integration and test program is well underway. The telescope was completed in the spring of 2016 and the cryogenic test equipment has been through two optical test programs leading up to the final flight verification program. The details of the telescope mirror integration will be provided along with the current status of the flight observatory. In addition, the results of the two optical ground support equipment cryo tests will be shown and how these plans fold into the flight verification program.

**Keywords:** JWST, Telescope, Integration, Test, Cryo

## 1. INTRODUCTION

The James Webb Space Telescope (Figure 1.1) is the successor to the Hubble Space Telescope. JWST will operate in the infrared region of the electromagnetic spectrum to allow the science community to observe far red shifted stars and galaxies as they were originally forming after the Big Bang 13.8 billion years ago. The scientists call JWST the first light machine since it will actually observe the first stars “turning on” and early galaxy formation. Even though the light from these early stars and galaxies was created billions of years ago, that light is just getting to our solar system now. They are moving away from us at nearly the speed of light Doppler-shifting the visible light into the infrared. In order to image this phenomenon, the telescope must also image in the infrared spectrum. This means that the telescope and all the systems that create that image must be very cold. That is why JWST operates at 40°K. This extreme temperature creates many challenges for the engineers and scientists that are building and testing the observatory. This paper will provide an overview of the Alignment, Integration, and Test (AI&T) program and provide specific details on the OTIS integration effort and the preparation for the final cryo test before the OTIS delivery to JSC.

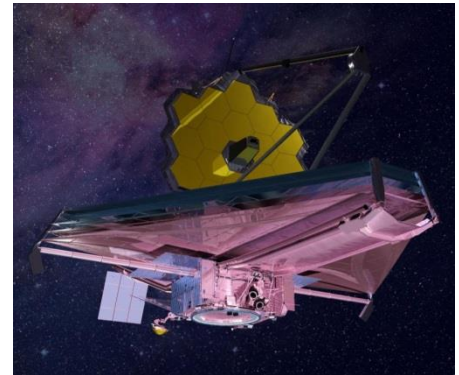


**Figure 1.1:** The James Webb Space Telescope in its fully deployed configuration.

## 2. OTIS INTEGRATION

The subsystems that will comprise the final observatory are completed. The Optical Telescope Element (OTE) integration has been discussed in paper 9904-2 in these conference proceedings. The Integrated Science Instrument Module also successfully completed its cryogenic verification test program. The next step is the completion of what is commonly called the OTIS (OTE plus ISIM). In reality, the ISIM is more than just the instruments. Figure 2.1 provides an overview of the three major components of the ISIM. The figure shows the ISIM that contains the physical instruments. There is also the IEC (ISIM Electronics Compartment) and the HR (Harness Radiator). The OTIS also has various thermal radiators and blankets that need to be installed in order to finalize the flight configuration.



**Figure 2.1:** The ISIM components are shown above. Upper left – ISIM instruments, Middle – Harness radiator, Bottom – ISIM Electronics compartment.



**Figure 2.2:** The completed OTE is shown in the assembly stand.

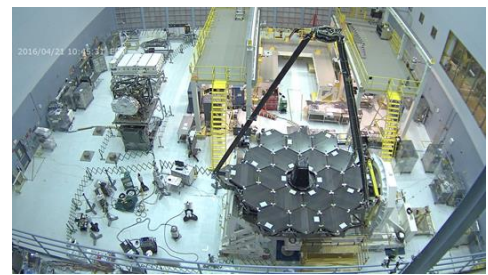


**Figure 2.3:** The OTE was moved from the assembly stand shown at the top of the photograph to the High Capacity Roll and Turnover Fixture. Some blanketing and radiator installation will occur here before being flipped over for ISIM integration.

To install the ISIM, the telescope needs to be flipped over to provide access to the rear of the Backplane Support Frame. In order to do that, the telescope is moved from the integration stand (Figure 2.2) over to the High Capacity Roll and Turnover Fixture (Figure 2.3). While in this configuration, thermal blankets and a large radiator are attached before the reach and access are blocked due to the ISIM installation and before being turned over, the protective covers that have covered the gold-coated mirrors have to be removed since they are merely sitting on the mirrors. The “big reveal” took place over two days with technicians removing the covers (Figure 2.4). Needless to say, this was a very exciting time for the JWST team and a proud moment for Dr. John Mather in the ultimate selfie in a reflection off the 18 segment primary mirror (Figure 2.5).



**Figure 2.4:** Before flipping over, the protective covers have to be removed by technicians on diving boards (left). The primary mirror, fully revealed, is finally visible (right).



**Figure 2.5:** Dr. John Mather’s reflection can be seen in the primary mirror.

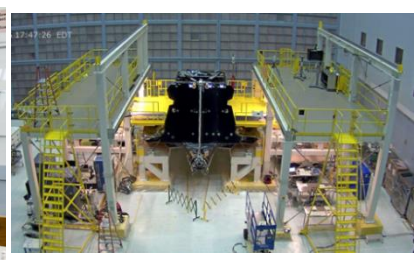


**Figure 2.6:** The OTE is shown rotated and placed back in the assembly stand in preparation for ISIM integration.

Once rotated with the primary mirror facing down, the OTE was placed back in the assembly stand (Figure 2.6) in preparation for the ISIM integration. Rolling platforms were included in the assembly stand to allow excellent reach and access behind the mirrors and into the ISIM cavity in the telescope backplane structure. A specially designed extendable diving board was also designed that actually extends through the telescope that allows access to the interior of the telescope structure. The ISIM will be attached to the telescope via six kinematic struts that are shown in Figure 2.7. These struts are adjustable in length allowing the ISIM to be aligned to the telescope. Critical metrology measurements provide the data to align the telescope and instrument pupil locations in zero gravity at cryo temperatures. To accomplish

this in gravity and room temperature, calibrated finite element models are used to bias the installation location so that the optimal alignment is achieved once on-orbit. Figure 2.8 shows the ISIM being installed into the telescope.



**Figure 2.7:** The ISIM instrument subsystem is attached to the telescope via six kinematic struts (Two monopods and two bipods). These struts are adjustable to allow the telescope and instrument pupils to be aligned.



**Figure 2.8:** The ISIM is carefully lowered into the telescope and attached via the 6 struts.

This paper did not allow the inclusion of the remaining subsystems prior to the publication date. The hardware is comprised mainly of thermal radiators and thermal management hardware and is staged and ready for installation per plan.

Once the OTIS is completed, it will go through a series of environmental tests at the Goddard Space Flight Center. This includes a pre and post center of curvature testing of the telescope with a three-axis vibration test and an acoustic test program to verify the ability to withstand the rigors of the launch to space. Once that is completed, the STTARS (Space Telescope Transporter for Air Road and Sea) shipping container (Figure 2.9) will be used to move the OTIS from Maryland to the Johnson Space Center in Houston, Texas. Once there, an end-to-end optical test will be done at the operating temperature in order to verify the on-orbit performance of the system.

In preparation for that critical test program, a series of tests using the JWST Pathfinder telescope has been ongoing for the past year. A series of three tests are planned prior to the OTIS test. Optical Ground Support Equipment (OGSE) Test #1 and #2 are complete. A final Thermal Pathfinder (TPF) test is planned to start late summer 2016.



**Figure 2.9:** Once completed, the STTARS shipping container will be used to move the system to the Johnson Space Center in Houston, Texas for the cryogenic optical test.

### 3. JSC ENVIRONMENTAL TEST SYSTEM

The cryogenic testing will take place at the Johnson Space Center (JSC) in Houston, Texas. The JSC Chamber A is a legacy vacuum chamber originally built for the Apollo program in the 1960's. This chamber was never intended to be an optical test chamber or a cryogenic test facility capable of creating a 20K test environment. Therefore, a major retrofit was in order that took several years to complete.

The basic chamber was fully functional and with its large 40-foot (12.2m) diameter door, it was really a perfect choice for JWST. Therefore, the original solar lamps that illuminated the Apollo Command Module (Figure 3.1) were removed and the existing liquid Nitrogen (LN2) shrouds were refurbished. While that was going on, an inner set of thermal shrouds were fabricated and installed that would support the gaseous Helium (GHe) cryogen enabling a 20K test

environment. Once that work was completed, it was time to start to install all the Optical Ground Support Equipment (OGSE) that will allow the ground test of the JWST OTIS.

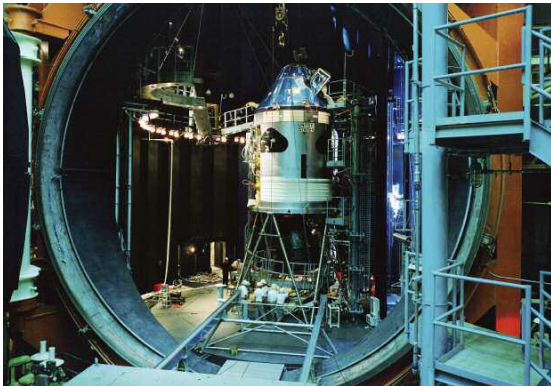


**Figure 3.1:** Chamber A was originally built to test Apollo spacecraft and has been refurbished for its new role to test JWST.

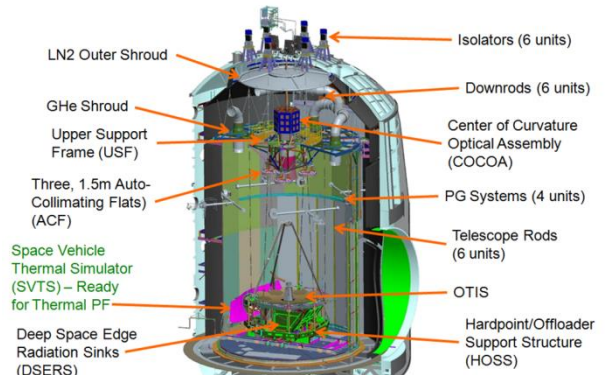


**Figure 3.2:** The JWST cryo test configuration is shown inside Chamber A.

Figure 3.2 is a CAD model of the chamber with the OGSE installed. A brief description of each major piece of OGSE will be discussed below:

- Starting at the top of the chamber, there are six isolators manufactured by Minus-K. These six isolators allow the test team to transform the very noisy Apollo vacuum chamber into a quiet environment capable of supporting a precision optical test program. These six isolators support a total suspended mass of about 60,000 pounds (27,000 kg).
- Connected to the isolators are six downrods. These downrods also make the transition from the external air environment to the internal vacuum environment via a set of stainless steel bellows. These downrods are vertical and reach down to suspend the optical test system below.
- The main support structure is called the Upper Support Frame (USF) and is shown in Figure 3.3. The USF provides interfaces for the Center of Curvature Optical Assembly (CoCOA), the three, 1.5m auto collimating flats (ACF's), and the six telescope rods that support the OTIS at the bottom of the chamber.



**Figure 3.3:** The Upper Support Frame (USF) is shown in the JSC clean room. The stepladder shown is 12 feet (3.7m) tall.



**Figure 3.4:** The Center of Curvature Optical Assembly (CoCOA) is shown at the Marshall Space Flight Center during early risk reduction testing. Note that the thermal panels have not yet been installed in this photo.

- The CoCOA (Figure 3.4) is one of the major optical test systems for the JWST cryo test. The essence of the CoCOA is basically a two element null and a 4D multiwavelength interferometer (MWIF). The MWIF allows the test team to quickly align and phase the segmented primary mirror. It also provides a full aperture evaluation of the primary mirror since we only sample the end-to-end system aperture through our three subaperture ACF's. There are various features within the CoCOA to aid in the identification and alignment of the primary mirror. See Reference 2 for a complete discussion of the CoCOA.
- The three ACF's are lightweight borosilicate mirrors manufactured by HEXTEK (Figure 3.5). Borosilicate was used for the ACF's since the operating temperature of the mirrors is at the zero coefficient of expansion (CTE) of the glass. Therefore, the surface figure is very stable at the cryo test temperatures. The ACF's are cryo null figured at the operating temperature prior to installation at JSC.

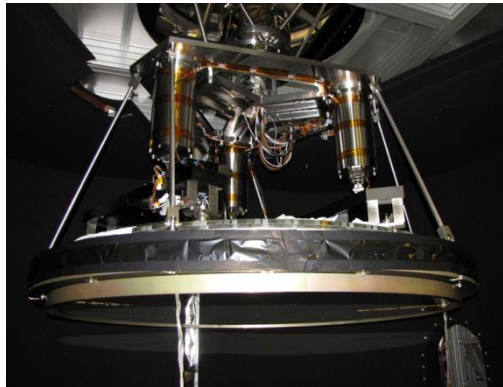


**Figure 3.5:** The ACF assembly is shown with the three-actuator assemblies suspending the 1.5m lightweight mirror underneath.



**Figure 3.6:** The Hardpoint/Offleader Support Structure (HOSS) is shown after painting. The structure is approximately 30 feet (9m) in length and width.

- There are six telescope rods that hang from the USF and support the Hardpoint/Offloader Support Structure (HOSS). The very large stainless steel structure (Figure 3.6) holds the flight OTIS in a kinematic configuration of two monopod struts on one end and two sets of bipods on the other end.
- There are four photogrammetry (PG) systems manufactured by Johns Hopkins University Instrument Development Group that are attached to the walls of the chamber (Figure 3.7). The camera systems inside pressure tight enclosures that are thermally controlled. Each system rotates in a windmill fashion through 360 degrees of rotation. This PG system allows the test team to understand where the hardware is in the chamber to about 100 microns.

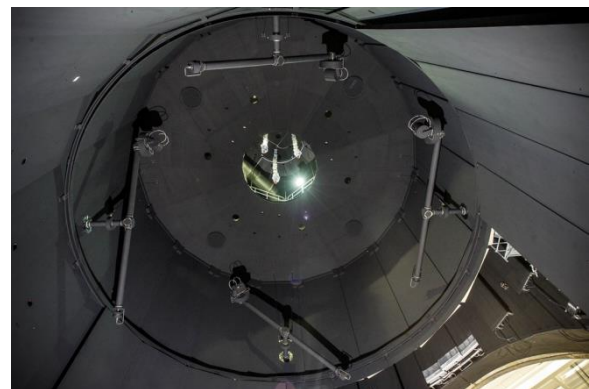


**Figure 3.7:** The four-photogrammetry systems are shown in their final "windmill" configuration in the JSC vacuum chamber.

This comprises the Optical Ground Support Equipment that will be used to test the flight OTIS. There is additional thermal ground support equipment that completes the test equipment suite. The thermal equipment is discussed in Section 5.

#### **4. OPTICAL GSE TEST PROGRAM RESULTS**

One of the main purposes of the Pathfinder telescope was to exercise all the test equipment, the test processes, and the test personnel; proving to be valuable experiential training for the upcoming test on the OTIS. The Pathfinder includes two Primary Mirror Segment Assemblies (PMSAs) and a Secondary Mirror Assembly (SMA) with nearly similar functions as the OTIS mirrors (Figure 4.1). A simulator for the Science Instruments, called the Beam Image Analyzer

(BIA), placed a near infrared detector array, similar to arrays in the Science Instruments, at the Pathfinder telescope focal surface on stages to allow translation in all directions and small tilts to allow placing the detector anywhere on the focal surface.

The Pathfinder optical tests consisted of two cryogenic test cycles. The first test cycle, OGSE 1, tested the full test configuration without the prime Aft Optical Assembly (AOS), which contains the fine steering mirror and the tertiary mirror. The second test cycle, OGSE 2, added the AOS and the AOS Source Plate Assembly (ASPA) with its optical point sources at the Cassegrain focus to allow the execution of all optical tests before delivering the AOS for integration into the OTE.

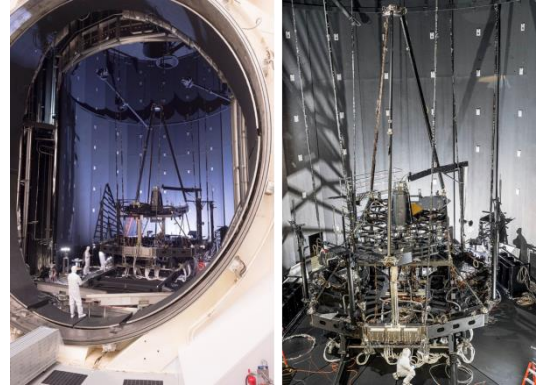


**Figure 4.1: Pathfinder telescope with flight AOS before second cryogenic test.**

The first order of business was to check alignments after a  $\sim 250^\circ\text{K}$  cool down. From photogrammetry measurements, the alignment of the primary mirror relative to the CoCOA and the ACFs were well within tolerance. The CoCOA allows 6 degrees of freedom, although clocking about the optical axis is not used. Table 4.1 shows the ample remaining adjustment range available after the cool down alignment shift for the CoCOA.

**Table 4-1: Remaining range of adjustment in the CoCOA after the alignment shift from the cool down.**

|                        | V1<br>(mm)    | V2<br>(mm)   | V3<br>(mm)   | RV1<br>( $\mu\text{rad}$ ) | RV2<br>( $\mu\text{rad}$ ) | RV3<br>( $\mu\text{rad}$ ) |
|------------------------|---------------|--------------|--------------|----------------------------|----------------------------|----------------------------|
| Range                  | +/- 24.6      | +/- 32       | +/- 32       | N/A                        | +/-5.6                     | +/-5.6                     |
| Cryo Position (margin) | -7.4<br>(70%) | 7.2<br>(76%) | 0.4<br>(98%) | -0.6                       | 0.5<br>(92%)               | -0.5<br>(90%)              |

The ACFs have adjustment in tilt to move the collimated beam to selected field angles and piston, though piston is not used. Knowledge of the decenter and clocking positions of the ACF optical surfaces is important to remove the ACF surface figure from the telescope’s images. The decenter position is also limited to prevent light leakage from adjacent PMSAs during Wavefront Sense and Control operations for the three PMSAs within the clear aperture of the ACF. The two Pathfinder tests only had one of the three ACFs installed – the ACF reflecting through the two PMSAs on the Pathfinder. The alignment and function of the other two ACFs will occur in the upcoming thermal test of the Pathfinder (Section 5 below). Table 4.2 shows the range margin for the tilt relative to the PM and the position margin for decenter relative to the PMSAs.

**Table 4-2: Remaining tilt range of adjustment in the ACF and the decenter position relative to tolerance after the alignment shift from the cool down.**

|                        | Decenter<br>(mm) | Tilt<br>(mrad) |
|------------------------|------------------|----------------|
| Range                  |                  | 10.8           |
| Cryo Position (margin) | (70%)            | 0.15<br>(99%)  |

Photogrammetry is then used to align the PM and SM relative to the AOS (Reference 14). The accuracy of the photogrammetry system was compared against laser tracker measurements prior to the cryogenic tests. The measured dimensions of Invar bars with measured coefficients of thermal expansion and the dimensions of the beryllium mirrors were checked against expectations at the cryogenic test temperatures. The repeatability at cryogenic temperatures was also determined (Reference 15). The results did reveal issues with the mechanical interface of a few of the photogrammetry targets with the PMSAs that will be resolved before the OTIS test. Table 4.3 shows the repeatability of the photogrammetry system. With this repeatability, Table 4.4 contains the accuracy of the measurements.

**Table 4-3: Example repeatability measurements with the photogrammetry system.**

|                  | 2σ M1 (mm) | 2σ M2 (mm) | 2σ M3 (mm) |
|------------------|------------|------------|------------|
| ACF              | 0.040      | 0.067      | 0.124      |
| SM               | 0.034      | 0.020      | 0.058      |
| ASPA support arm | 0.047      | 0.021      | 0.022      |
| ASPA             | 0.021      | 0.007      | 0.008      |
| AOS-Base         | 0.020      | 0.015      | 0.013      |
| PM               | 0.023      | 0.010      | 0.014      |
| Strut Base       | 0.116      | 0.024      | 0.053      |

**Table 4-4: Photogrammetry accuracy.**

| Hardware component | Measurement | Requirement | Predicted (mm or mrad) | Margin (%) |
|--------------------|-------------|-------------|------------------------|------------|
| PM-AOS (TRD-342)   | PISTON      | 0.1 mm      | 0.038                  | 62         |
|                    | DECENTER    | 0.1 mm      | 0.084                  | 16         |
|                    | TILT        | 0.15 mrad   | 0.090                  | 40         |
|                    | CLOCKING    | 1 mrad      | 0.309                  | 69         |
| SM-AOS (TRD-347)   | PISTON      | 0.15 mm     | 0.086                  | 43         |
|                    | DECENTER    | 1.25 mm     | 0.652                  | 48         |
|                    | TILT        | 0.335 mrad  | 0.274                  | 24         |

With the PMSAs and SM globally aligned to the AOS, the PMSAs are then aligned and phased to within a piston error of 32 nm for best wavefront error (WFE) (Reference 16). The WFE matched model prediction within the uncertainty of the measurement and the model at 31 nm RMS WFE – see Figure 4.2 for the WFE of the inner segment.

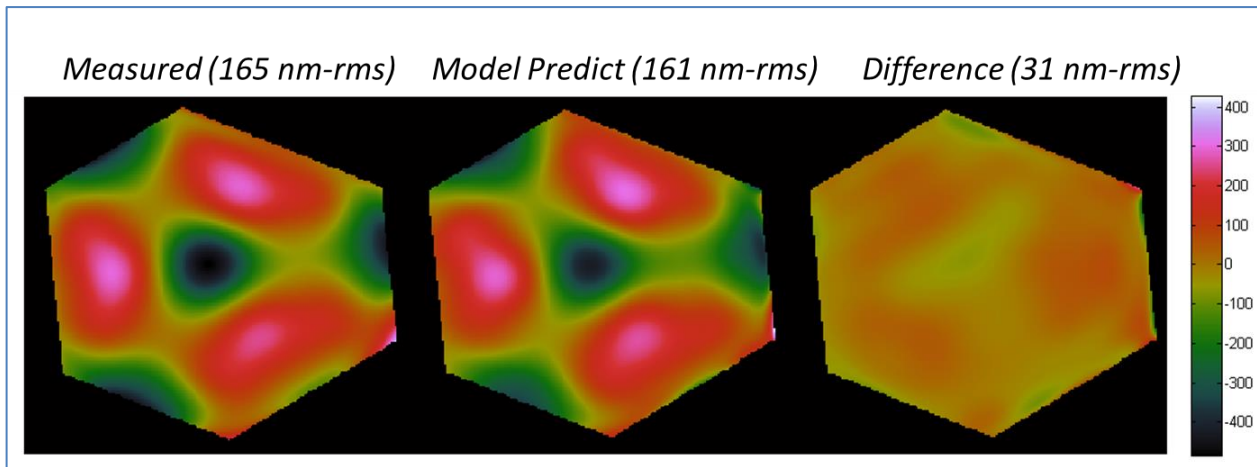


**Figure 4.2: Measured WFE of inner PF mirror segment compared to model prediction – the triad error results from the radius of curvature actuator compensation of the gravity sag of the light weighted mirror.**

Next, the BIA was placed relative to the AOS focal surface at multiple field positions using calibration metrology, gravity analysis, and photogrammetry. Then the detector position was compared to the best focus position of the images from the inward optical sources on the ASPA (Figure 4.3 and Table 4.5). The comparison averaged across the field positions agreed to within 0.435 mm along the focal direction and within 0.166 mm laterally, approximately half of the value of the expected uncertainty.

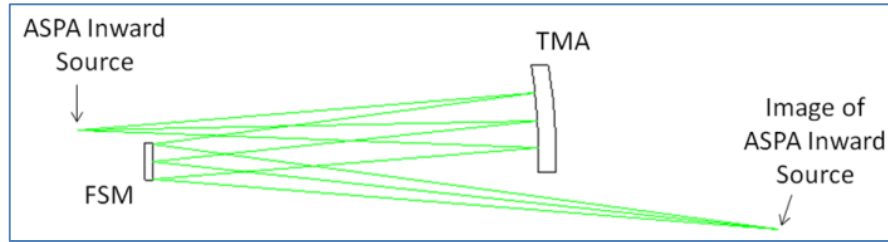


Figure 4.3: ASPA Inward source is imaged by AOS and best focus position compared to detector position set by photogrammetry.

Table 4-5: Comparison of image location based in phase retrieval analysis of image vs. expected location based on metrology and finite element model predictions.

| Instrument FOV | ASPA Source Designation | Best Image Location |          |          | Metrology Location |          |          | PRMS - Prediction |          |          |
|----------------|-------------------------|---------------------|----------|----------|--------------------|----------|----------|-------------------|----------|----------|
|                |                         | M1 (mm)             | M2 (mm)  | M3 (mm)  | M1 (mm)            | M2 (mm)  | M3 (mm)  | dM1 (mm)          | dM2 (mm) | dM3 (mm) |
| NIRCamB        | I-1                     | -1809.338           | -41.378  | -325.920 | -1810.325          | -41.515  | -325.799 | 0.987             | 0.137    | -0.120   |
| NIRCamB        | I-3                     | -1811.261           | -34.780  | -332.990 | -1811.839          | -34.835  | -332.594 | 0.578             | 0.055    | -0.395   |
| NIRCamB        | I-4                     | -1811.047           | -34.666  | -332.468 | -1811.839          | -34.835  | -332.594 | 0.792             | 0.168    | 0.127    |
| NIRCamA        | I-5                     | -1808.646           | 89.324   | -347.837 | -1809.430          | 88.997   | -347.686 | 0.784             | 0.327    | -0.151   |
| NIRCamA        | I-6                     | -1808.681           | 88.822   | -347.878 | -1809.430          | 88.997   | -347.686 | 0.749             | -0.176   | -0.192   |
| FGS1           | I-7                     | -1790.147           | 156.513  | -462.293 | -1790.725          | 156.482  | -462.090 | 0.579             | 0.030    | -0.204   |
| FGS1           | I-8                     | -1791.067           | 163.177  | -462.404 | -1791.598          | 163.164  | -462.228 | 0.531             | 0.013    | -0.176   |
| FGS1           | I-9                     | -1793.820           | 163.421  | -469.502 | -1793.987          | 163.321  | -469.287 | 0.167             | 0.099    | -0.215   |
| FGS2           | I-11                    | -1793.662           | -15.854  | -462.467 | -1794.608          | -15.915  | -462.375 | 0.946             | 0.060    | -0.092   |
| FGS2           | I-13                    | -1796.089           | -9.200   | -469.493 | -1796.959          | -9.269   | -469.399 | 0.870             | 0.069    | -0.094   |
| NIRISS         | I-15                    | -1786.456           | -216.090 | -456.663 | -1786.327          | -216.140 | -456.396 | -0.129            | 0.051    | -0.267   |
| NIRISS         | I-16                    | -1783.960           | -215.915 | -449.566 | -1784.044          | -215.989 | -449.378 | 0.084             | 0.074    | -0.188   |
| MIRI           | I-23                    | -1808.903           | -277.834 | -238.417 | -1808.916          | -278.029 | -238.552 | 0.013             | 0.195    | 0.135    |
| MIRI           | I-24                    | -1809.133           | -277.921 | -238.937 | -1808.916          | -278.029 | -238.552 | -0.217            | 0.108    | -0.385   |
| NIRSPEC        | I-25                    | -1803.834           | 292.103  | -271.288 | -1804.099          | 292.001  | -271.097 | 0.265             | 0.102    | -0.191   |
| NIRSPEC        | I-26                    | -1805.759           | 298.933  | -271.463 | -1805.724          | 298.839  | -271.217 | -0.035            | 0.094    | -0.247   |
| Average        |                         |                     |          |          |                    |          |          | 0.435             | 0.088    | -0.166   |
| StdDev         |                         |                     |          |          |                    |          |          | 0.410             | 0.103    | 0.144    |
| Range          |                         |                     |          |          |                    |          |          | 1.204             | 0.503    | 0.530    |

These measurements also provided a measurement of the AOS WFE for each field point to compare to the model prediction. The comparison varied between 9 and 40nm RMS WFE across the seven measured field points – less than the variation between alternative analysis software.

The Secondary Mirror focus position was set by using an upward source on the ASPA to retro-reflect from the auto-collimating flat mirror near the top of the chamber to form an image on the BIA detector, and then moving the SM to set the focus to the detector position. Due to higher than expected vibration of the primary mirror segments, the images from the two segments required separation to analyze the images without confusion from the vibration effect. By calibrating the relative tilt positions of the segments with the CoCOA, a Hartmann analysis could be used to determine focus and other lower order image quality measurements (Reference 17) nearly as well as stable phased PMSAs within the ACF subaperture (Figure 4.4).

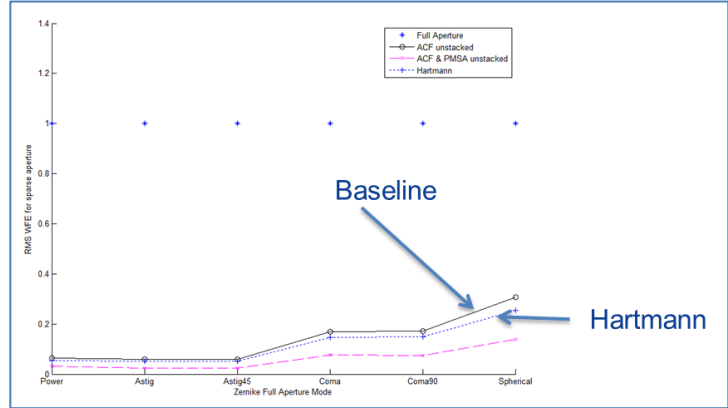


Figure 4.4: Sensitivity of Hartmann configuration of the PMSAs compared to the baseline approach of phased mirror segments.

Other parameters were measured including the PM collection area with an interferometer camera image, practice of the radius of curvature measurement with a Leica Absolute Distance Meter, and plate scale by tilting the ACF and a PMSA. The alignment of the primary mirror to the pupil mask near the Fine Steering Mirror in the AOS is accomplished by using linear arrays of LEDs at the PM edge and detecting which LEDs pass through the mask to reach the BIA detector. The LED locations are determined using metrology, finite element model predictions, and photogrammetry. Since the LED light does not pass through the PMSAs, this image is similar to the flight test. Figure 4.5 has a schematic of the LED locations and the test image of the LEDs that passed through the mask. The BIA has a second detector with a singlet lens to create the pupil image. Table 4.6 shows the nominal vs. actual alignment measured in the Pathfinder. The result was a measured 0.3% pupil shear from the nominal alignment.

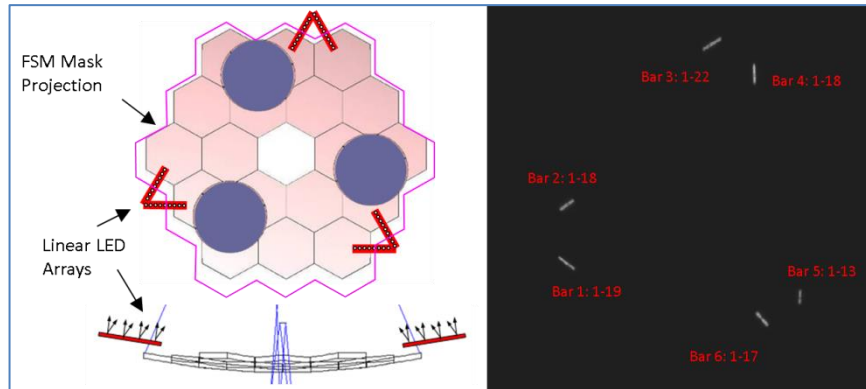


Figure 4.5: Schematic of linear LED array locations relative to primary mirror. Light emits towards the Secondary Mirror.

Table 4-6: Schematic of linear Led array locations relative to primary mirror. Light emits towards the Secondary Mirror.

| Bar                      | 1  | 2  | 3  | 4  | 5  | 6  |
|--------------------------|----|----|----|----|----|----|
| Nominal Last visible LED | 20 | 18 | 21 | 17 | 13 | 16 |
| Actual last visible LED  | 19 | 18 | 22 | 18 | 13 | 17 |

Finally, an important test checked all the light paths through the ASPA structure and the AOS aperture in the cryogenic vacuum environment. This establishes a baseline image for the OTIS test. Any deviations in the image during the OTIS test can be confidently attributed to the structure between the AOS and the instrument detectors. This image is created using the LEDs mentioned above as a source. Since the LEDs are at a pupil conjugate, the imaged light (without a pupil imaging lens) spreads across the detector plane at the focal conjugate. Figure 4.6 shows the test image from the Pathfinder test.

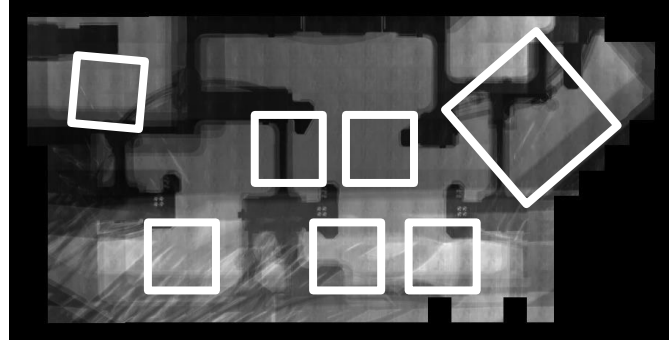


Figure 4.6: Image created by scanning the BIA detector without a pupil imaging lens through the field using light from some LEDs used in the pupil alignment test.

## 5. PLANS FORWARD TO OTIS CRYO TEST

As the OTIS integration, work continues at GSFC in the SSDIF clean room, work is progressing to finalize the configuration for the Thermal Pathfinder (TPF) test at JSC. The Pathfinder has been fitted with thermal blankets and mirror simulators (Figure 5.1) to replicate as well as possible the flight configuration of the OTIS.



Figure 5.1: The Pathfinder has been fitted with mirror simulators for the Pathfinder thermal test. The HOSS is shown on the left side of the photograph.

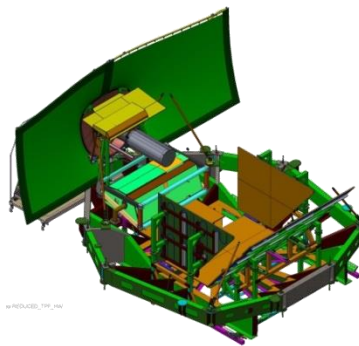


Figure 5.2: The DSERS and SVTS are shown on the HOSS. The flight system sits inside these thermal components to simulate the flight environment at L2.

The ground support equipment is also being fitted with all the additional thermal hardware that was not needed for OGSE#1 and OGSE#2. This includes the Space Vehicle Thermal Simulator (SVTS) and Deep Space Edge Radiator Systems (DSERS) that are shown in the Figure 5.2 CAD drawing. Basically, the OTIS sits in a tub of specially designed actively cooled radiators that mimic the space environment. The SVTS simulates the spacecraft bus and the transition from the warm sun facing side to the cold observatory side.

The TPF test will allow the test team to actually practice the cool down and observe the steady state environment that will be used for the flight OTIS. In addition, the performance of the thermal system can be evaluated to insure that the provided environment will provide the rigorous test program parameters required to insure that the OTIS would operate as expected at L2.

## 6. SUMMARY

The OTIS AI&T program is progressing per plan. The OTIS integration is well underway at the Goddard Space Flight Center and the final Pathfinder cryo test is being configured for later this summer.

The OTIS cryo test is less than a year away!

## REFERENCES AND RELATED PAPERS

- [1] **Optomechanical Integration and Alignment Verification of the James Webb Space Telescope (JWST) Optical Telescope Element**  
Conrad Wells, Matthew Coon, ITT Space Systems Division (United States)  
Published in Proceedings Volume 7433: August 2009
- [2] **The Center of Curvature Optical Assembly for the JWST Primary Mirror Cryogenic Optical Test: Optical Verification**  
Conrad Wells, Gene Olczak, Cormic Merle, Tom Dey, Mark Waldman, Tony Whitman, Eric Wick, Aaron Peer, ITT Corp. Geospatial Systems (United States)  
Published in Proceedings Volume 7790: August 2010
- [3] **Architecting a Revised Optical Test Approach for JWST**  
Charlie Atkinson, Jonathan Arenberg, Northrop Grumman (United States); Gary Matthews, Mark Waldman, Alan Wertheimer, Tony Whitman, ITT (United States); Jim Oschmann, Ball Aerospace & Technologies Corp. (United States)  
Published in Proceedings Volume 7010: August 2008
- [4] **The Center of Curvature Optical Assembly for the JWST Primary Mirror Cryogenic Optical Test**  
Conrad Wells, Gene Olczak, Cormic Merle, Tom Dey, Mark Waldman, Tony Whitman, Eric Wick, Aaron Peer, ITT Geospatial Systems (United States)  
Published in Proceedings Volume 7739: July 2010
- [5] **JWST's Cryogenic Position Metrology System**  
Tony L. Whitman, ITT Exelis Geospatial Systems (United States); Randolph P. Hammond, Joe Orndorff, Stephen Hope, Stephen A. Smee, The Johns Hopkins Univ. (United States); Thomas Scorse, Keith A. Havey, Jr., ITT Exelis Geospatial Systems (United States)  
Published in Proceedings Volume 8442: August 2012
- [6] **The Integration and Test Program of the James Webb Space Telescope**  
Randy A. Kimble, Pamela S. Davila, Charles E. Diaz, Lee D. Feinberg, Stuart D. Glazer, NASA Goddard Space Flight Ctr. (United States); Gregory S. Jones, Northrop Grumman Aerospace Systems (United States); James M. Marsh, NASA Goddard Space Flight Ctr (United States); Gary W. Matthews, ITT Exelis Geospatial Systems (United States); Douglas B. McGuffey, NASA Goddard Space Flight Ctr. (United States); Patrick H. O'Rear, NASA Johnson Space Flight Ctr. (United States); Deborah D. Ramey, NASA Goddard Space Flight Ctr. (United States); Carl A. Reis, NASA Johnson Space Flight Ctr. (United States); Scott C. Texter, Northrop Grumman Aerospace Systems (United States); Tony L. Whitman, ITT Exelis Geospatial Systems (United States)  
Published in Proceedings Volume 8442: August 2012
- [7] **Assembly Integration and Ambient Testing of the James Webb Space Telescope Primary Mirror**  
Conrad Wells, Tony Whitman, John Hannon, Art Jensen, Eastman Kodak Co. (United States)  
Published in Proceedings Volume 5487: October 2004
- [8] **Integration and Verification of the James Webb Space Telescope**  
Charles B. Atkinson, Pat Harrison, Northrop Grumman Corp. (United States); Gary Matthews, Eastman Kodak Co. (United States); Paul Atcheson, Ball Aerospace & Technologies Corp. (United States)  
Published in Proceedings Volume 5180: December 2003

- [9] **James Webb Space Telescope System Cryogenic Optical Test Plans**  
Lee D. Feinberg, NASA Goddard Space Flight Ctr. (United States); Allison Barto, Ball Aerospace & Technologies Corp. (United States); Mark Waldman, Sigma Space Corp. (United States); Tony Whitman, ITT Corp. Geospatial Systems (United States)  
Published in Proceedings Volume 8150: September 2011
- [10] **James Webb Space Telescope Primary Mirror Integration: Testing the Multiwavelength Interferometer on the Test Bed Telescope**  
Gene Olczak, David J. Fischer, Mark Connelly, Conrad Wells, ITT Corp. Geospatial Systems (United States)  
Published in Proceedings Volume 8146: September 2011
- [11] **James Webb Space Telescope (JWST) Optical Telescope Element (OTE) Pathfinder Status and Plans**  
Lee D. Feinberg, Ritva A. Keski-Kuha, NASA Goddard Space Flight Ctr. (United States); Charles B. Atkinson, Northrop Grumman Aerospace Systems (United States); Andrew J. Booth, Sigma Space Corp. (United States); Tony L. Whitman, Exelis Geospatial Systems (United States)  
Published in Proceedings Volume 9143: Space Telescopes and Instrumentation 2014: Optical, Infrared, and Millimeter Wave: September 2014
- [12] **JWST Telescope Integration and Test Status**  
Gary W. Matthews, Thomas R. Scorse, Scott Kennard, John Spina, Tony Whitman, Exelis Inc. (United States); Scott Texter, Charles Atkinson, Greg Young, Northrop Grumman Aerospace Systems (United States); Ritva A. Keski-Kuha, James M. Marsh, Juli Lander, Lee D. Feinberg, NASA Goddard Space Flight Ctr. (United States)  
Published in Proceedings Volume 9143: Space Telescopes and Instrumentation 2014: Optical, Infrared, and Millimeter Wave: September 2014
- [13] **Use of a Pathfinder Optical Telescope Element for James Webb Space Telescope Risk Mitigation**  
Lee D. Feinberg, Ritva Keski-Kuha, NASA Goddard Space Flight Ctr. (United States); Charlie Atkinson, Scott C. Texter, Northrop Grumman Aerospace Systems (United States)  
Published in Proceedings Volume 7731: Space Telescopes and Instrumentation 2010: Optical, Infrared, and Millimeter Wave: July 2010
- [14] **Alignment Test Results of the JWST Pathfinder Telescope Mirrors in the Cryogenic Environment**  
Whitman, T.L., Wells, C., Hadaway, J., Knight, J.S., Lunt, S., Proc. SPIE 9904-161, (2016)
- [15] **Model Predictions and Observed Performance of JWST Cryogenic Position Metrology System**  
Lunt, S., et. al., Proc. SPIE 9904-166, (2016)
- [16] **Performance of the Primary Mirror Center-of-Curvature Optical Metrology System During Cryogenic Testing of the JWST Pathfinder Telescope**  
Hadaway, J.B., et. al., Proc. SPIE 9904-150, (2016)
- [17] **Hartmann Test for the James Webb Space Telescope**  
Knight, J.S., et. al., Proc. SPIE 9904-11, (2016)